Int. J. Electron. Commun. (AEÜ) 170 (2023) 154786

Contents lists available at ScienceDirect

International Journal of Electronics and Communications

journal homepage: www.elsevier.com/locate/aeue

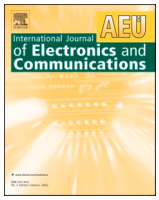

Regular paper

An improved FSK-modulated class-E power and data transmitter for biomedical implants

Farshad Gozalpour, Mohammad Yavari *

Integrated Circuits Design Laboratory, Department of Electrical Engineering, Amirkabir University of Technology (Tehran Polytechnic), P.O. 15875-4413, Tehran 15914, Iran

ARTICLE INFO

Keywords:
Frequency-shift keying (FSK)
Dual-resonance inductive link
Inductive power and data transmission
Biomedical implant

ABSTRACT

This paper presents an efficient dual-resonance biomedical inductive link for frequency-shift keying (FSK) modulation. In this link, the combination of PCB coil as the main coil and the solenoid as the compact inductance creates a dual-resonance coil. 3.22 mm of winding diameter in solenoid makes the link suitable for biomedical implants. Using the dual-resonance link, an efficient FSK-modulated power and data transmitter is proposed for biomedical implants to transmit power and data simultaneously with the same carriers and a single inductive link. So, there is no concern about the interference between power and data carriers. Also, the presence of two resonance frequencies at the secondary side of the link significantly improves the efficiency. With a 6 mm air gap and 2.5 Mbps data rate (DR), the measured power delivered to load (PDL) and power transmission efficiency (PTE) are 57.4 mW and 48.4%, respectively. Also, with a 6 mm interface of beef ribs + medical-grade silicone, the measured PDL and PTE are 48.2 mW and 38.8%, respectively. The measured bit error rate (BER) for 2.5 Mbps data rate is less than 10^{-5}.

1. Introduction

Nowadays, wireless power transmission (WPT) is essential for a continuous and safe operation of implantable medical devices (IMDs), and inductive coupling is the oldest and predominant WPT strategy that can provide the required power with high reliability, safety, and efficiency [1–6]. Power transmission efficiency (PTE) is an important parameter in evaluation of inductively coupled systems. By increasing PTE, the external battery life-time is increased and the maximum allowable amount of AC magnetic field passing through tissue is observed. An essential solution in increasing PTE is to use LC resonance structures with a resonance frequency equal to the driver frequency. At this frequency, the impedance of the LC tanks is pure resistive without any reactive term.

In WPT systems, the simultaneous achievement of high efficiency continuous power transmission along with a high data rate (DR) is a challenging issue. This challenge becomes even more difficult in modulations such as frequency-shift keying (FSK) that require two carriers. To alleviate this challenge, the power and data transmission links can be separated (separate coupling interfaces), and each of them can be designed to meet the desired needs. In these architectures, the amplitude of power carrier is much more than that of data carrier, resulting in reduced signal-to-noise ratio (SNR) at the data receiver coil [7]. In order to minimize the restrictions on design of data filter and prevent possible data signal saturation even before entering the filter, a reliable telemetry system must eliminate this interference. Various implementations have been proposed to reduce these interferences such as coplanar and coaxial [7], orthogonal [8], and figure-eight [9]. However, due to misalignments and limited space, the interference and cross-talk will not be completely removed. Also, large space of implanted coils is another major disadvantage of the multi-link systems.

These disadvantages encourage designers to transfer power and forward data using only one inductive link (one coupling interface). In this architecture, the same carrier (or carriers) is utilized to transmit data and power, simultaneously. Therefore, there is not any interference between the power and data carriers. In [10], an FSK-modulated data and power transmitter is proposed where the capacitor of the load network as well as the capacitor parallel to the switch of power amplifier (PA) are switched according to input “0” and “1” data. This is done to keep the PA tuned at both carrier frequencies of FSK modulation. This mechanism has been used just in transmitter side and it cannot be used at the secondary side because the receiver is not informed of input data

* Corresponding author.
E-mail address: myavari@aut.ac.ir (M. Yavari).

https://doi.org/10.1016/j.aeue.2023.154786
Received 12 March 2023; Accepted 11 June 2023
Available online 16 June 2023

before its reception. Thus, the secondary side of the link has only one resonance frequency, and the PTE is only equal to 25%. In [11], using the combination of series and parallel LC tanks in primary side of the link, two resonance frequencies are obtained, but the secondary side has only one resonance frequency and the PTE is as low as 24%. Also, in [11], no attempt has been made for optimal operation of the PA at both carrier frequencies of FSK modulation. In summary, the presence of only one resonance frequency at the secondary side of FSK-modulated transmitter links in [10] and [11] has reduced the PTE.

The dual-resonance coil is an attractive method to create dual-resonance links. However, the previous works [12,13] have not been designed for biomedical implants. For example, in [12], the diameter of the coils is 20 cm, which is not suitable for biomedical implants. In [12], only the efficiency analysis has been performed, and the ability of a dual-resonance link in simultaneous transmission of power and data, which is an important issue in biomedical applications, has not been investigated. Also, the dual-resonance based power and data transmitter in [13] has been designed for high power and very low DR ($\leq$0.02 Mbps) requirements.

In this paper, the focus is mainly on the architecture of biomedical inductive link for simultaneous transmission of power and data in FSK mode using only one inductive link. In order to mitigate the trade-off between the efficiency and bandwidth, a dual-resonance inductive link is implemented for cochlear implants. In this link, the PCB circular coils make the coupling interface, and the combination of compact solenoids (with winding diameter of 3.22 mm and winding length of 9.46 mm) with PCB coils results in two resonance frequencies, which is necessary for FSK-modulation. Then, using the dual-resonance link, a power and data transmitter is implemented for cochlear implants where the drain waveforms of class-E PA satisfy the tuned operation at both carrier frequencies of FSK-modulation. The performance of transmitter is measured in two different intermediate interfaces of air, and beef ribs + silicone. While achieving DR of 2.5 Mbps and data rate to carrier frequency (DRCF) ratio of 33.3%, the PTE of transmitter is improved due to the presence of two resonance frequencies at the secondary side of the link.

The rest of paper is organized as follows. Section 2 presents the dual-resonance inductive link for biomedical implants, as well as the calculated electrical parameters of PCB coil and solenoid. In Section 3, the simulation and measurement results of inductive link are reported. In Section 4, FSK-modulated class-E power and data transmitter is presented. Finally, the measurement results of power and data transmitter and conclusion are given in Sections 5 and 6, respectively.

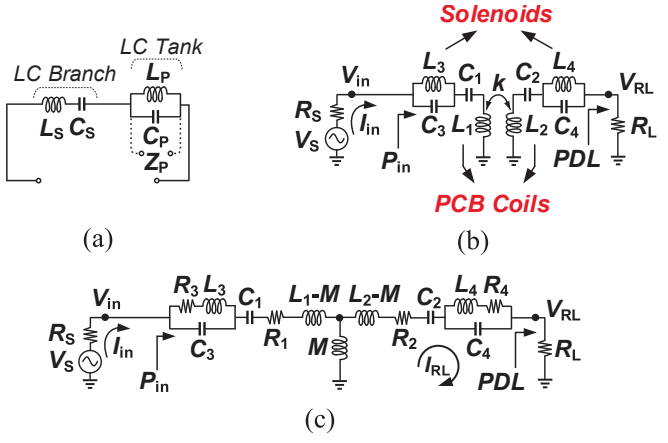

Fig. 1. (a) Dual-resonance coil, (b) dual-resonance inductive link, (c) T-model of inductive link.

2. Biomedical dual-resonance inductive link

Fig. 1(a) shows the equivalent circuit of a dual-resonance coil, which is made of LC branch and LC tank, and has two resonance frequencies. The capacitor C_S is connected to the main coil L_S to achieve the LC branch. LC tank is obtained by parallel combination of capacitor C_P and compact inductance L_P. When the operating frequency is lower than the resonance frequency of LC tank, it operates inductively (Z_P is inductive), and when the operating frequency is higher than its resonance frequency, it operates capacitively. The low resonance frequency (f_{o1}) is achieved by combination of LC branch and inductive LC tank, and the high resonance frequency (f_{o2}) is achieved by the combination of LC branch and capacitive LC tank as [12]:

$$f_{o1} = f_{oLC1}\sqrt{0.5+\left(\frac{r_C}{2}\right)\left(1+r_L-\sqrt{\left(\frac{r_L r_C-1}{r_C}\right)^2+2\left(\frac{r_L r_C+1}{r_C}\right)+1}\right)}$$
$$f_{o2} = f_{oLC1}\sqrt{0.5+\left(\frac{r_C}{2}\right)\left(1+r_L+\sqrt{\left(\frac{r_L r_C-1}{r_C}\right)^2+2\left(\frac{r_L r_C+1}{r_C}\right)+1}\right)} \quad (1)$$

where f_{oLC1} is the resonance frequency of LC branch, $r_L = L_S/L_P$, and $r_C = C_S/C_P$ in Fig. 1(a). f_{oLC2} is the resonance frequency of LC tank, which is equal to $\sqrt{r_c r_L} \times f_{oLC1}$. Both f_{oLC1} and f_{oLC2} have to be placed between f_{o1} and f_{o2}. The resulting bandwidth allows both carriers of FSK modulation to pass through the link with a sufficient energy transmission to the load.

Fig. 1(b) shows the schematic of dual-resonance inductive link with dual-resonance coils. $L_{1,2}$ are PCB coils with coupling coefficient of k, and $L_{3,4}$ are compact solenoids. In Fig. 1(c), in order to obtain the link parameters, the coupled coils L_1 and L_2 are replaced with equivalent T-model, where M is the mutual inductance and R_1, R_2, R_3, and R_4 are the series resistances of L_1, L_2, L_3, and L_4, respectively. In Fig. 1(c), by assuming $L_1 = L_2 = L$, $L_3 = L_4 = L/r_L$, $C_1 = C_2 = C$, $C_3 = C_4 = C/r_C$, $R_1 = R_2 = R_{PCB}$ (PCB coil resistance), $R_3 = R_4 = R_{Sol}$ (solenoid resistance), $M = k(L_1L_2)^{1/2} = kL$, and $C = 1/(L(2\pi f_{oLC1})^2) = 1/(L(\omega_{oLC1})^2)$, I_{in} and I_{RL} are given by:

$$I_{in} = \frac{V_s b}{ab+(\omega M)^2}, \quad I_{RL} = \frac{V_s}{-j\omega M + ab/(j\omega M)} \quad (2)$$

where

$$a = R_s + R_{PCB} + j\omega L + \frac{L(\omega_{oLC1})^2}{j\omega} + \frac{R_{Sol}+j\omega(L/r_L)}{1-\frac{\omega^2}{r_L r_C(\omega_{oLC1})^2}+j\frac{\omega R_{Sol}}{Lr_C(\omega_{oLC1})^2}} \quad (3)$$

The expression for b is similar to a ($b = a - R_S + R_L$). At resonance frequencies of the link, f_{o1} and f_{o2}, the imaginary terms in (3) cancel each other, and only the real terms will remain as:

$$a = R_s + R_{PCB} + \frac{R_{Sol}}{(1-\frac{\omega^2}{r_L r_C(\omega_{oLC1})^2})^2+(\frac{\omega R_{Sol}}{Lr_C(\omega_{oLC1})^2})^2} \quad (4)$$

With extracted a and b, I_{in}, I_{RL}, $V_{in} = V_s - R_s I_{in}$, and V_{RL} are calculated. The power delivered to the load (PDL) and the power drawn from the sinusoidal input source (P_{in}) can be calculated as:

$$PDL = \frac{R_L(I_{RL-pp})^2}{8} = \frac{V_{RL-pp}^2}{8R_L},$$
$$P_{in} = \frac{V_{in-pp} \times I_{in-pp}}{8} cos(\varphi - \theta) \quad (5)$$

where (φ-θ) is the phase shift between V_{in} and I_{in}. Also, $I_{RL\text{-}pp}$, $V_{RL\text{-}pp}$, $I_{in\text{-}pp}$, and $V_{in\text{-}pp}$ are the peak-to-peak values of I_{RL}, V_{RL}, I_{in}, and V_{in}, respectively. As mentioned before, f_{oLC1} and f_{oLC2} have to be placed between f_{o1} and f_{o2}. Assuming f_{o1} = 5 MHz and f_{o2} = 10 MHz as the resonance frequencies of inductive link, geometric averages of f_{o1} and f_{o2}

has been used as f_{oLC1} and f_{oLC2} ($\sqrt{f_{o1}f_{o2}} = 7.071MHz$). According to these values and relation (1), values of 2 and 0.5 are obtained for r_L and r_C, respectively. Considering these achieved values, PCB coils and compact solenoids are used as the main coils $L_{1,2}$, and compact inductances $L_{3,4}$, respectively.

2.1. Electrical parameters

In this section, electrical parameters of the PCB coils and solenoids are calculated. Fig. 2 shows the geometric parameters of PCB coils $L_{1,2}$, and solenoids $L_{3,4}$. In PCB coils, the parameters D_{out}, D_{in}, W, S, and n are outer diameter, inner diameter, trace width, trace spacing, and number of turns, respectively. The thickness of the conductor layer in PCB is considered to be 35 μm. In solenoids, D, d, p, l, and n represent the winding diameter, wire diameter, winding pitch, winding length, and number of turns, respectively. $D = 3.22$ mm and $l = 9.46$ mm, make the solenoid suitable for implantation in body.

The electrical model of the coils includes inductance, AC series resistance, and parallel capacitance. For the PCB circular coils, the inductance can be determined by [14]:

$$L = \frac{\mu_0 n^2 d_{avg}}{2}\left[\ln(2.46/\beta) + 0.2\beta^2\right] \tag{6}$$

where $\mu_0 = 4\pi \times 10^{-7}$ H/m is the permeability of free space, $d_{avg} = 0.5(D_{out} + D_{in})$ is the average diameter, and $\beta = (D_{out}\text{-}D_{in})/(D_{out} + D_{in})$ is the fill-factor. Using (6), 3.1 μH is obtained for PCB coils $L_{1,2}$ with reported parameters in Fig. 2.

The inductance of solenoids is given by [15]:

$$L = \frac{\mu_0 \pi r^2 n^2 \kappa}{l} \tag{7}$$

Where k is the Nagaoka's coefficient [15], and $r = D_{eff}/2$. D_{eff} is the effective winding diameter [16], which can be interpolated from empirical Medhurst data table [17]. The result for solenoids $L_{3,4}$ with reported parameters in Fig. 2 is 1.65 μH.

The skin effect is the main source of AC resistance which is caused by high frequency currents. For PCB coils, the skin effect loss, R_{skin}, is given by [14]:

$$R_{skin} = R_{DC}\frac{t_c}{\delta(1-\exp(-t_c/\delta))}\frac{1}{1+t_c/W}, \quad \delta = \sqrt{2\rho/\omega\mu_0} \tag{8}$$

where t_c is the conductor thickness (35 μm), δ is the skin depth, $\rho = 1.72 \times 10^{-8}$ Ω.m is the resistivity of copper, and $R_{DC} = \rho l_C/A$ is the DC resistance. $l_C = n\,\pi\,d_{avg}$ is the conductor length. R_{skin} for PCB coils $L_{1,2}$ at 5 MHz and 10 MHz is 1.72 Ω and 2.08 Ω, respectively.

For solenoids, the AC resistance is given by [17]:

$$R_{ac} = \frac{\rho l_w}{\pi(d\delta - \delta^2)}\Phi\frac{n-1}{n}, \quad l_w = \sqrt{(n\pi D_{eff})^2 + l^2} \tag{9}$$

where l_w is the effective wire length, and Φ is the proximity factor which can be interpolated from empirical Medhurst data table. Using (9), R_{ac} for solenoids $L_{3,4}$ at 5 MHz and 10 MHz is 1.47 Ω and 1.98 Ω, respectively.

In [18], an approximation for parasitic capacitance of PCB coils is given as:

$$C_p \approx (x\varepsilon_{rc} + y\varepsilon_{rs})\varepsilon_0\frac{t_c}{S}l_g \tag{10}$$

where ε_{rc} and ε_{rs} are the relative dielectric constants of coating layer and substrate, respectively. l_g is the length of gap between traces and it is approximately equal to:

$$l_g = 2\pi\sum_{i=1}^{n-1}\left(\left(D_{out}/2\right) - iW - (i-0.5)S\right) \tag{11}$$

For the case of air and FR-4 PCB, we have $(x, y) = (0.9, 0.1)$ and $(\varepsilon_{rc}, \varepsilon_{rs}) = (1, 4.4)$ [18]. Using (10), the parasitic C_p of 0.889 pF is obtained for PCB coils $L_{1,2}$.

Medhurst formula gives a simple expression for the self-capacitance of solenoids in pF/cm as [19]:

$$\left(C/D\right) = 0.1126\left(l/D\right) + 0.08 + 0.27\sqrt{\left(D/l\right)} \tag{12}$$

The calculated value for $L_{3,4}$ is 0.57 pF/cm. It is worth mentioning that Medhurst formula overestimates the parasitic capacitance for the solenoids with small l/D.

3. Simulation and measurement results of inductive link

In this section, PCB coils and solenoids with reported geometries in Fig. 2 have been fabricated and the setup of Fig. 3 is employed to measure the link parameters. PCB coils are implemented on FR-4 PCB with substrate thickness (t_s) of 1.6 mm, and magnet wire is used for solenoids.

The load resistance R_L is 50 Ω, $V_{s\text{-}pp} = 11$ V, and $R_s = 55$ Ω is the series combination of function generator 50 Ω resistance and a 5 Ω resistor. This 5 Ω resistor is required to measure the I_{in}. In order to establish the same conditions for simulations and measurements, the R_s resistance of 55 Ω is also considered in the simulations. Rohde & Schwarz HMO2022 and GW Instek AFG-2225 are employed as oscilloscope and function generator, respectively. After measuring $I_{in\text{-}pp}$, $V_{in\text{-}pp}$, $V_{RL\text{-}pp}$, and also the phase shift (φ-θ) between V_{in} and I_{in}, the relation (5) is utilized to extract the P_{in}, PDL, and PTE of inductive link. It is worth mentioning that $I_{in\text{-}pp}$, $V_{in\text{-}pp}$, and $V_{RL\text{-}pp}$ are the peak-to-peak values of I_{in}, V_{in}, and V_{RL}, respectively. In addition to the link parameters, the Wayne Kerr 6550P high frequency LCR meter with the 1J1011 fixture connected to the front panel BNC sockets is employed for the measurement results of inductance and AC resistance in PCB coils and solenoids.

It is worth mentioning that in simulations of this section, 2-dimentional (2-D) axisymmetric modelling in COMSOL Multiphysics has been used for PCB coils and solenoids. These modellings and the utilized meshing are illustrated in Fig. 4 and Fig. 5. For a proper estimation of the skin effect, a boundary layer mesh has been used for the boundaries in cross-section of the turns. With these modellings, the number of required

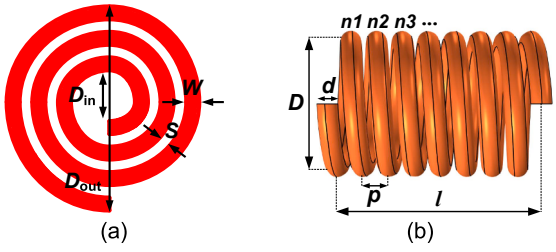

Parameter	D_{out} [mm]	D_{in} [mm]	W [mm]	S [mm]	n
PCB Coils $L_{1,2}$	25.5	11.1	0.3	0.3	12
Parameter	D [mm]	d [mm]	p [mm]	l [mm]	n
Solenoids $L_{3,4}$	3.22	0.2	0.22	9.46	43

Fig. 2. Geometric parameters of (a) PCB coils $L_{1,2}$, (b) solenoids $L_{3,4}$.

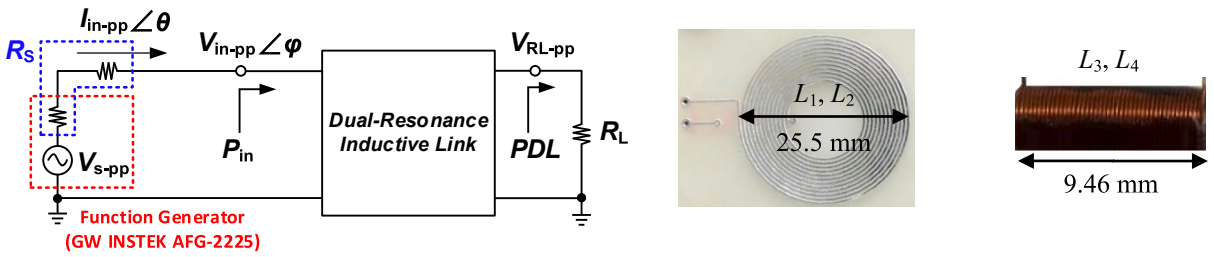

Fig. 3. Measurement setup of link parameters in dual-resonance inductive link.

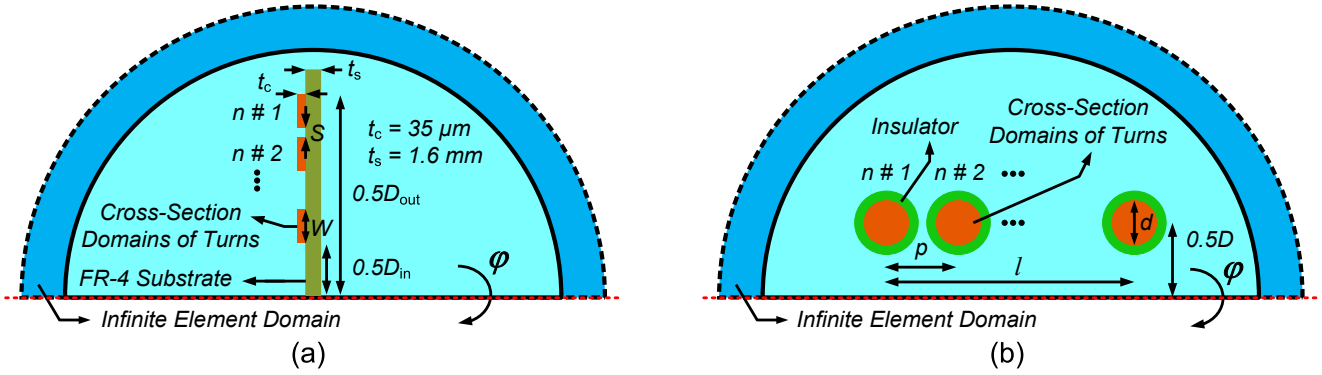

Fig. 4. 2-D axisymmetric modeling in COMSOL environment. (a) circular PCB coil, (b) solenoid.

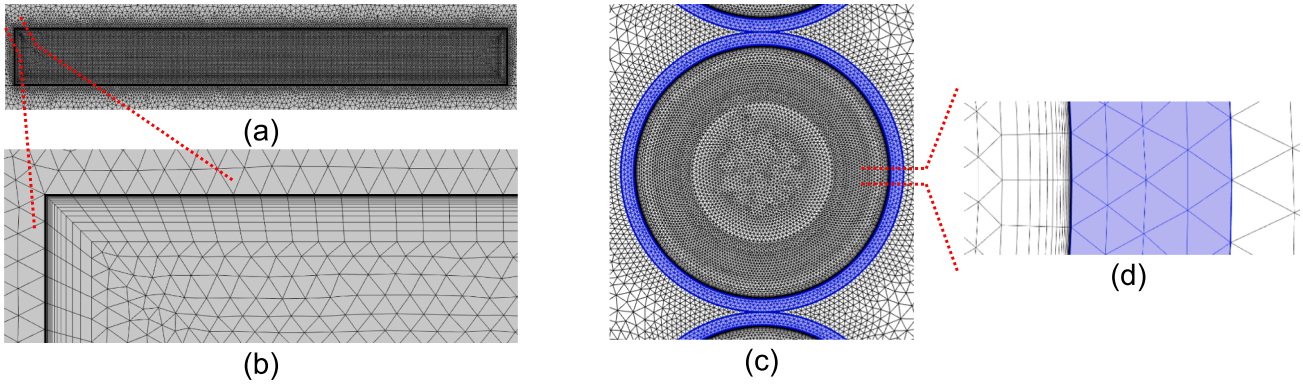

Fig. 5. Meshing and boundary layer of (a, b) rectangular cross-section domain of PCB coil, (c, d) circular cross-section domain of solenoid.

meshes in finite element method is reduced, which significantly decreases the extraction time of parameters.

Fig. 6(a) and Fig. 6(b) show the measured, simulated, and calculated inductance and AC resistance in the range of 1 MHz to 30 MHz for PCB coils $L_{1,2}$ and solenoids $L_{3,4}$, respectively. There is a good agreement between the measurement results, 2-D modelling based simulation results, and the calculation results from the previous relations. According to the measurement results, $L_{1,2}$ at 5 MHz and 10 MHz is about 3.15 μH, and $L_{3,4}$ at 5 MHz and 10 MHz is about 1.55 μH, and therefore $r_L = L_{1,2} / L_{3,4} \approx 2$. The simulated self-resonance frequency (f_{SRF}) of PCB coils for ε_{rs} of 1 and 4.4, and solenoids for ε_{ri} of 1, 2, and 4 are shown in Fig. 7(a) and Fig. 7(b), respectively. ε_{rs} and ε_{ri} are the relative dielectric constant of substrate in PCB coils and insulator layer in solenoids, respectively. The zero-crossing point specifies f_{SRF}. As ε_r increases, this point moves to lower frequencies, indicating a direct relation of ε_r with parasitic capacitances.

Fig. 8(a) shows the simulated PDL of link as a function of coupling coefficient (k) and frequency. Also, the simulated PTE of link, which is defined as the ratio of delivered power to the load, to the power drawn from the AC input source (PDL/P_{in} in Fig. 3), is shown in Fig. 8(b) as a function of k and frequency. Proportionality of PTE with k is well known. Also, at resonance frequencies of 5 MHz and 10 MHz, the stored reactive power in system is minimized, and therefore, high efficiency is achieved. The simulated PDL at 5 MHz and 10 MHz for $k = 0.31$ (simulated k for separation of 6 mm between PCB coils $L_{1,2}$) is 50.4 mW and 52.2 mW, respectively. The simulated PTE at 5 MHz and 10 MHz for $k = 0.31$ is 68.7% and 87.8%, respectively. By applying the simulation conditions in relations (2)-(5), the same results are obtained for the PDL and PTE of link in calculations, and therefore, the simulation results and calculation results verify each other.

Fig. 9 shows the measured and simulated results of PDL and PTE at 5 MHz and 10 MHz for separation of 3 mm to 12 mm. At both frequencies, the PDL is an increasing function of separation to some extent, and then it is decreased. In other words, for a particular separation, the condition of maximum power transfer to the load is met. For the separation of 6 mm, the measured PTE at 5 MHz and 10 MHz is 66.2% and 84.7%, respectively. Also, the measured PDL at 5 MHz and 10 MHz is 48.9 mW and 50.1 mW, respectively.

For the separation of 5 mm, 6 mm, and 7 mm between PCB coils, the frequency is swept from 3.5 MHz to 15 MHz and the measured PDL and

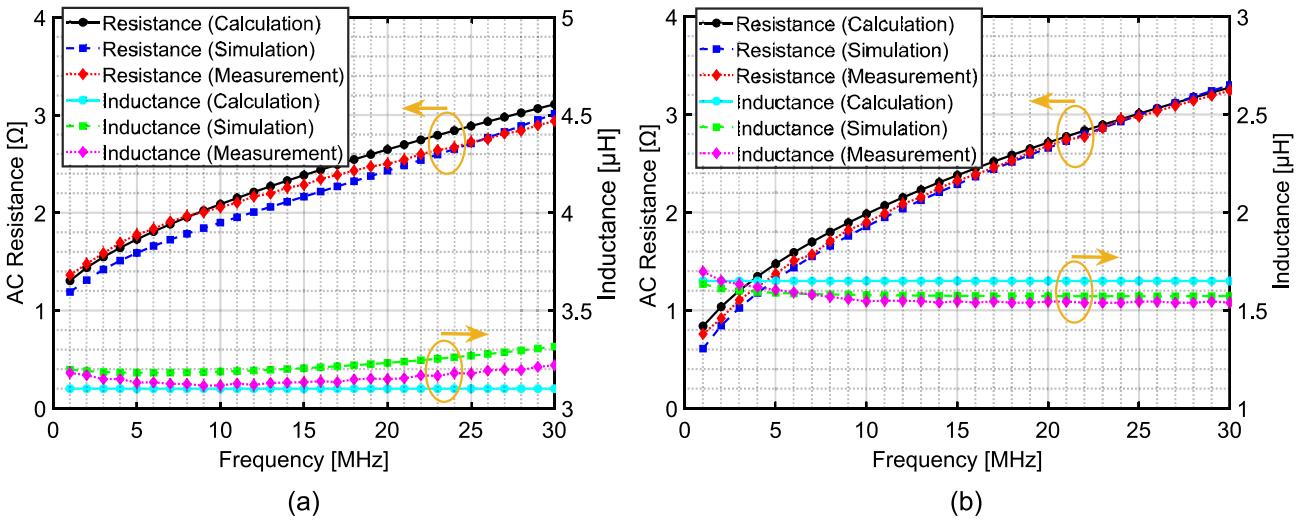

Fig. 6. Inductance and AC resistance of (a) PCB coils $L_{1,2}$, (b) solenoids $L_{3,4}$.

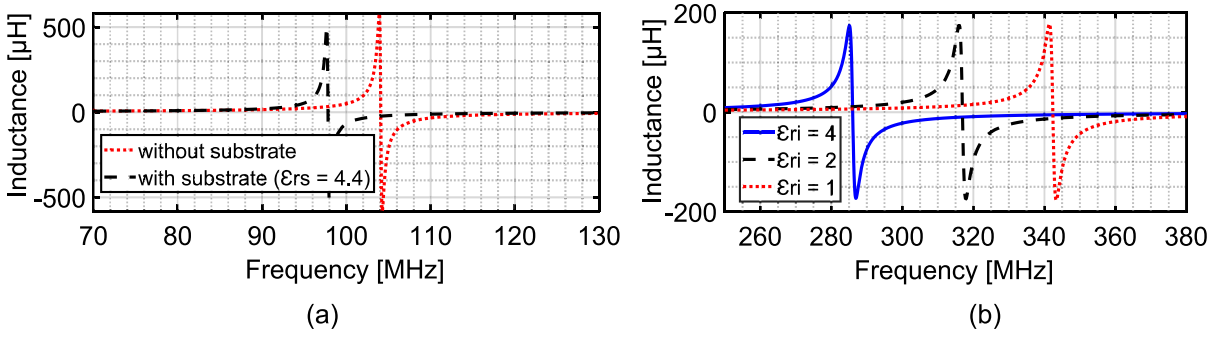

Fig. 7. Simulated self-resonance frequency of (a) PCB coils $L_{1,2}$, (b) solenoids $L_{3,4}$.

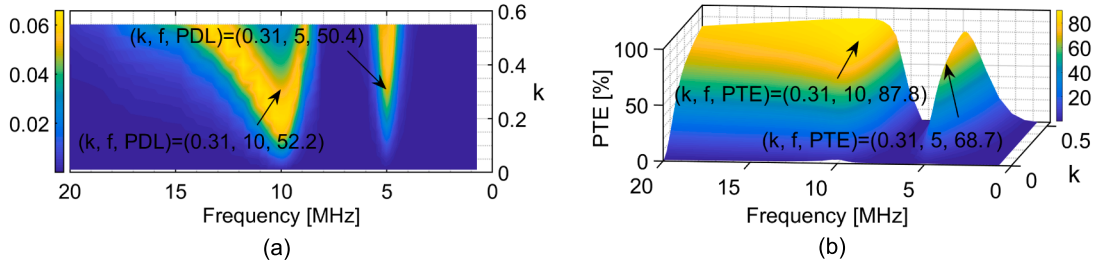

Fig. 8. Simulated (a) PDL, (b) PTE of the inductive link.

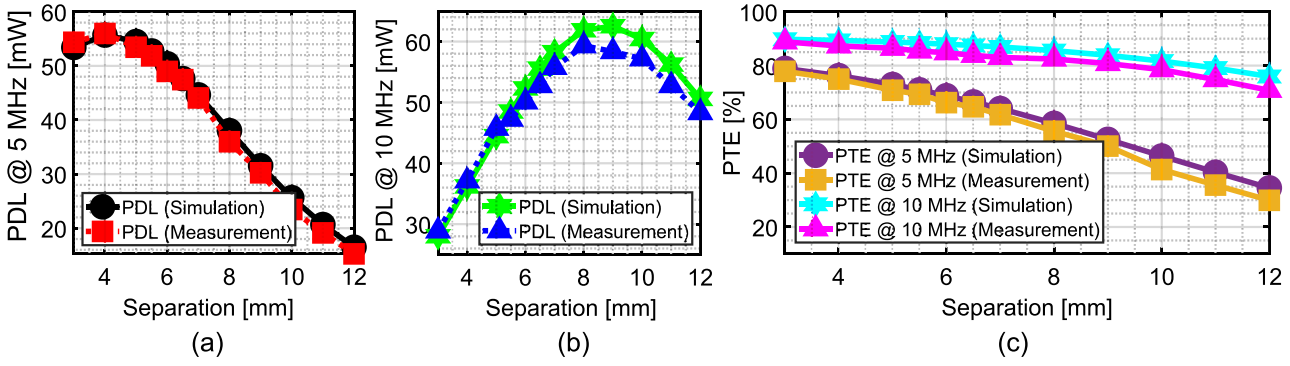

Fig. 9. Inductive link measured and simulated (a) PDL at 5 MHz, (b) PDL at 10 MHz, (c) PTE at 5 MHz and 10 MHz.

PTE of the link is reported in Fig. 10. It is observed that the obtained PTE at resonance frequencies (5 MHz and 10 MHz) is higher than other frequencies.

4. Biomedical power and data transmitter

Fig. 11 shows the FSK-modulated power and data transmitter where a dual-resonance inductive link is used. It is well known that by reducing the frequency, heat loss of body tissue is also reduced. On the other hand, since in our transmitter, power and data are transmitted with the same carriers, reducing the frequency also reduces the data rate (DR). Therefore, carrier frequencies should be selected so that both the desired DR and low heat loss can be realized. In [20], it is claimed that if the frequency is set below 20 MHz, power loss of tissue can be disregarded. So, we choose the carrier frequencies to be lower than 20 MHz. The next important parameter is the data rate to carrier frequency (DRCF) ratio. The PA's quality factor (Q) goes up as the carrier frequencies are increased. With a higher Q, voltages and currents in the inductive link network require more periods to reach a new level. As a result, a linear increase in DR will no longer occur with increasing frequency, and DRCF ratio will be reduced. Based on the iterative simulations, 5 MHz and 10 MHz are selected as carrier frequencies of FSK modulation to achieve 2.5 Mbps DR and 33.3% DRCF ratio.

According to the conceptual waveforms in Fig. 11, a 10 MHz CLK is fed to a DFF based frequency divider to produce ½ CLK (5 MHz). To generate the FSK signal (V_{FSK}), a 2:1 MUX selects one of 10 MHz and 5 MHz CLKs for the pseudorandom data ($Data_{in}$) of "0" and "1", respectively [10]. $Data_{in}$ is a 2^5-1 pseudorandom bit stream with no more than five "0"s or "1"s in a row, which is generated by a 5-bit shift register with feedback. This feedback is created by XORing the outputs of 5th and 2nd stages and feeding that into the least significant bit. Also, in order to prevent any unwanted high frequency glitch at the gate of M_{E1}, DFF7 is utilized to synchronize the generated pseudorandom data with clock signal. The produced FSK signal is then fed to gate driver 1 (LM5114BMF) to generate the driving FSK waveform (V_{G1}) required by the main switch of PA (M_{E1}). A 60 V N-channel trench MOSFET 2N7002NXAK is used as M_{E1} which its input capacitance is as low as 15 pF, and reduces the power dissipation of gate driver.

It is known that if the class-E PA meets zero voltage switching (ZVS) and zero voltage derivative switching (ZVDS) conditions, it can achieve high efficiency. In order to fulfill these conditions at both carrier frequencies of FSK modulation, two parallel capacitors C_{p1} and C_{p2} are used, which C_{p2} is connected or disconnected by M_{E2} based on whether $Data_{in}$ is "1" or "0", respectively. Therefore, the parallel capacitor of M_{E1} is variable for $Data_{in}$ of "0" and "1". On the other hand, the LC tank of link (L_3, C_3), that is in series with LC branch (L_1, C_1), has capacitive or inductive behavior depending on whether the carrier frequency is 10 MHz or 5 MHz, respectively, which causes a variable series capacitance. So, by selecting appropriate values, the class-E PA can be tuned at both carrier frequencies of FSK modulation. For L_1, it should be noted that as it increases, the reflected impedance from the secondary to primary side is increased, which increases the PTE. Of course, by increasing L_1, Q of the link network will be also increased, resulting a lower DR. Therefore, a value must be chosen for L_1 to have a balance between DR and PTE.

Depending on the application, the implantable medical devices have a wide range of power requirement. The required power can be in the range of low (e.g. less than 1 mW for pacemakers [21]) to high (e.g. > 1 W for ventricular assist device (VAD) [22]). Our target in this paper is the cochlear implant. Depending on the electrode count, architecture of stimulator, stimulation current of electrodes, etc., the required power of cochlear implants can be in the range of 20 mW to 50 mW and higher [23–25]. In this paper, it is assumed that the required PDL of the cochlear implant is equal to 50 mW (depending on the architecture of cochlear implant and its requirements, the PDL can have a higher or lower value). It also has been assumed that implant requires the supply voltage of 1.8 V. Besides, LDO regulators have a voltage drop of 100 mV to 200 mV, and the voltage conversion ratio of about 80% is achievable for the rectifier. Therefore, the amplitude of voltage across the load (V_{RL} in Fig. 11) should be about 2.5 V. So, the required PDL can be modelled as R_L of 62.5 Ω ($62.5 = 2.5^2/(2 \times 50 \times 10^{-3})$).

At the receiver side, two resonance frequencies are produced by combination of LC tank (L_4, C_4) and LC branch (L_2, C_2), that results in high efficiency. The resonance frequencies are set to 5 MHz and 10 MHz. According to the conceptual waveforms in Fig. 11, for data demodulation, V_{RL} is fed to a comparator that converts it to a digital FSK signal (V_{Comp}). Then, this signal is delivered to a delay-cell to generate its delayed version ($V_{Comp\text{-}D}$). For a correct data detection, the delay value must be in the range of $(2f_{o2})^{-1}$ to $(2f_{o1})^{-1}$, where f_{o1} and f_{o2} are 5 MHz and 10 MHz, respectively. The delay value is set to 75 ns, which is the average of allowable range, to make the data detection resistant against non-idealities. Finally, a DFF is used and V_{Comp} is sampled by $V_{Comp\text{-}D}$ to detect $Data_{out}$. To recover CLK_{out}, first, $V_{Comp\text{-}D}$ is fed to a frequency divider to produce ½ $V_{Comp\text{-}D}$. Then, a 2:1 MUX is used to select one of $V_{Comp\text{-}D}$ and ½ $V_{Comp\text{-}D}$ according to $Data_{out}$ [26].

Fig. 12 shows the CMOS TSMC 180-nm implementation of modulator and demodulator in transmitter, where the architecture is the same as the commercial off-the-shelf (COTS) modulator and demodulator in Fig. 11. The modulator and demodulator are implemented with 3.3 V and 1.8 V transistors, respectively. The rest of transmitter is assumed to be on PCB. During the transmission of pseudorandom bit stream with data rate of 2.5 Mbps, the simulated power dissipation of CMOS modulator and demodulator is only 0.49 mW and 0.41 mW, respectively.

5. Measurement results of power and data transmitter

In order to measure the performance of transmitter, it is implemented with commercial off-the-shelf (COTS) products, and the cross section of two measrement setups are shown in Fig. 13, where PCB coils are facing each other. In setup I (Fig. 13(a)), there is a 6 mm air gap as an intermediate interface between the coils. FR-4 substrate with thickness of 1.6 mm is a mechanical support for copper traces of the coils. Cochlear implants are sealed hermetically with biocompatible materials and surrounded by tissue. In [27], it is claimed that the mean thickness of scalp (skin, dermis, and epidermis layers) for men and women is 3.24 mm and 2.35 mm, respectively. To emulate the scalp tissue as an

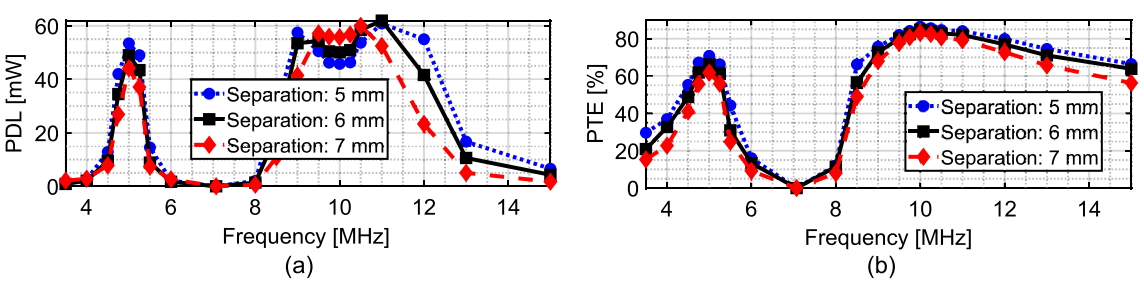

Fig. 10. Inductive link measured (a) PDL, (b) PTE for 3.5 MHz to 15 MHz.

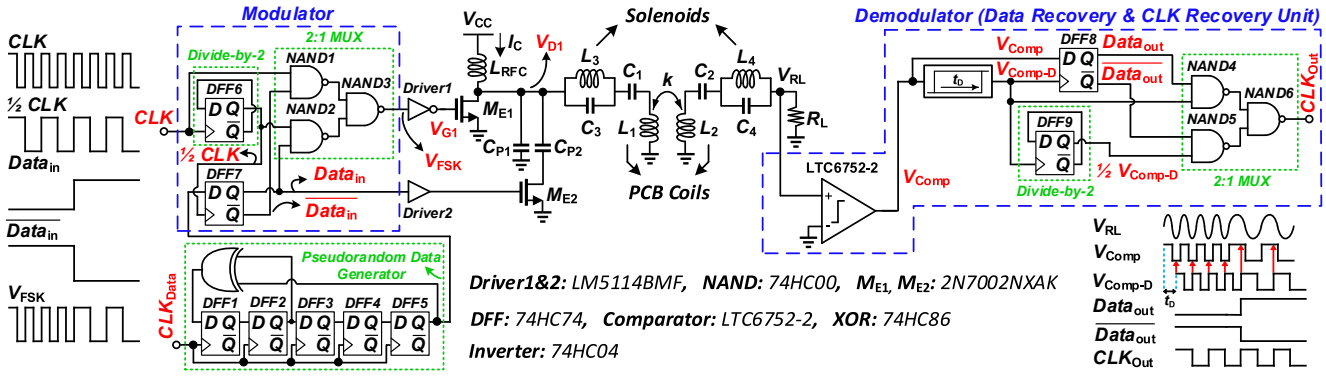

Fig. 11. Power and data transmitter implemented with dual-resonance inductive link.

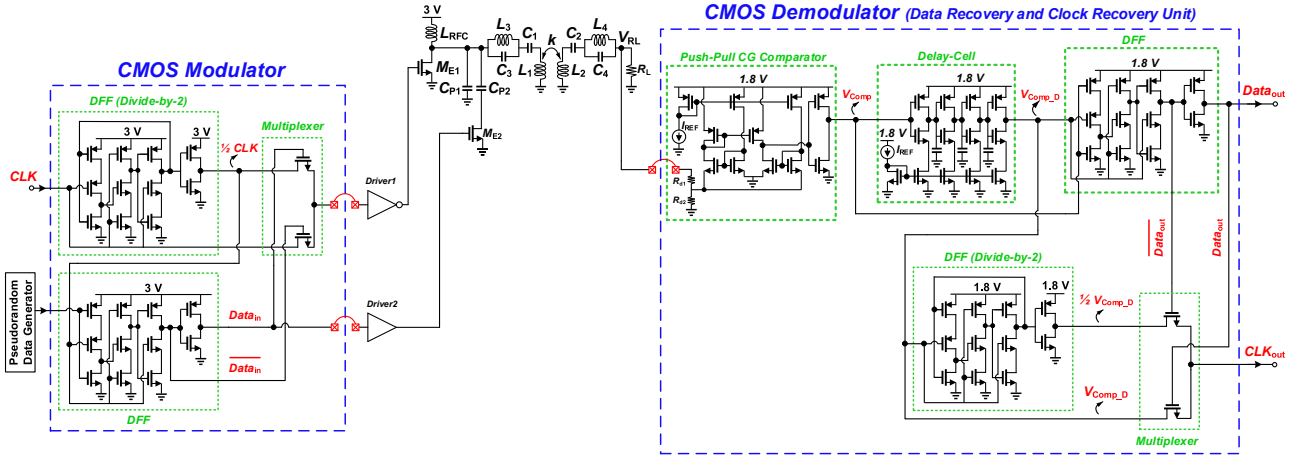

Fig. 12. CMOS implementation of modulator and demodulator in transmitter.

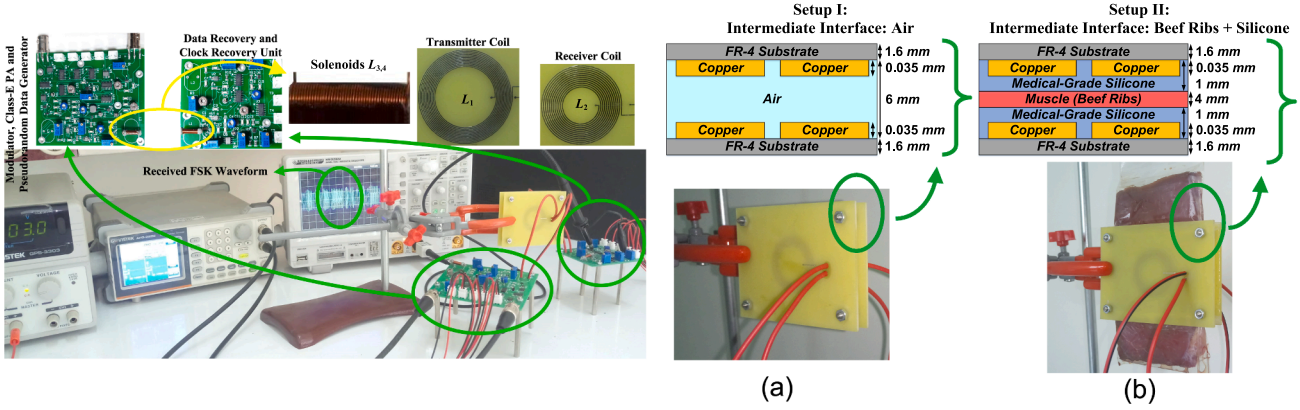

Fig. 13. Measurement setups of power and data transmitter. (a) setup I: intermediate interface of air, (b) setup II: intermediate interface of beef ribs + silicone.

interface in setup II (Fig. 13(b)), a ribs portion of beef with thickness of 4 mm is packaged in a polyethylene bag. Also, medical-grade silicone with 1 mm thickness is used as the biocompatible coating layers for PCB coils, which is necessary to insulate the implanted coil from tissue and fluids.

It should be noted that ε_r of muscle is high (100 to 200 [28]), which increases the parasitic capacitance, and decreases the self-resonance frequency of PCB coils if it is in direct contact with coils. On the other hand, ε_r is much lower for silicone (about 3 [29]), which minimizes the tissue effect on coils.

In both setups I and II, the transmitter is tuned for the separation of 6 mm between the coils, and component values and geometric parameters are reported in Table 1 and Table 2. In most of cochlear implants like Nucleus 7, the outer diameter (D_{out}) of the coils is limited to about 30 mm, which has been taken into account in this paper (Table 2). Fig. 14 shows the steady state waveforms of drain and gate voltages of M_{E1} for 6 mm separation between the coils. Fig. 14(a) and Fig. 14(b) are for setup I at 10 MHz and 5 MHz, respectively. Also, Fig. 14(c) and Fig. 14(d) are for setup II at 10 MHz and 5 MHz, respectively. These results show that the PA satisfies the tuned operation in all cases.

The demodulated 2.5 Mbps data and the recovered clock in setup I are illustrated in Fig. 15. To measure the BER, separation of PCB coils is

Table 1
Component values of power and data transmitter in setups I and II.

Comp.	Value		Comp.	Value	
	Setup I	Setup II		Setup I	Setup II
	Interface: Air	Interface: Beef Ribs + Silicone		Interface: Air	Interface: Beef Ribs + Silicone
V_{CC}	3 V	3 V	C_2	160 pF	160 pF
R_L	62.5 Ω	62.5 Ω	C_3	296 pF	315 pF
L_{RFC}	12 μH	12 μH	C_4	327 pF	327 pF
C_{P1}	32 pF	44 pF	L_1	5.2 μH	5.2 μH
C_{P2}	178 pF	193 pF	L_2	3.15 μH	3.15 μH
C_1	165 pF	172 pF	$L_{3,4}$	1.55 μH	1.55 μH

Table 2
Geometric parameters of PCB coils $L_{1,2}$ and solenoids $L_{3,4}$ in setups I and II.

Parameter	L_1	L_2	Parameter	L_3	L_4
D_{out}	29 mm	25.5 mm	D	3.22 mm	3.22 mm
D_{in}	18.15 mm	11.1 mm	d	0.2 mm	0.2 mm
W	0.25 mm	0.3 mm	p	0.22 mm	0.22 mm
S	0.2 mm	0.3 mm	l	9.46 mm	9.46 mm
n	12	12	n	43	43

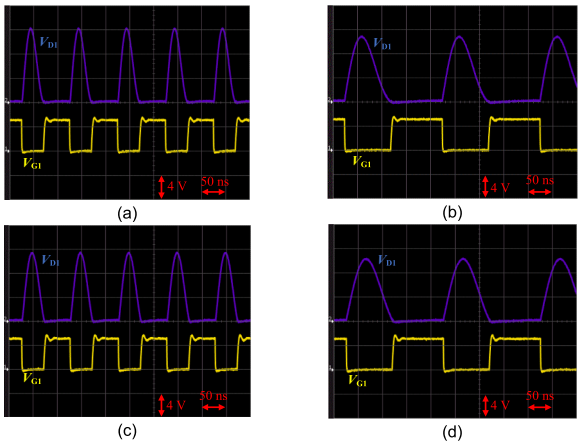

Fig. 14. Measured drain and gate voltage of M_{E1}. (a,b) setup I, (c,d) setup II.

set to 6 mm in both setups I and II. Then, a 2^5-1 pseudorandom bit stream is transmitted with DR of 2.5 Mbps, and it is demodulated at the receiver side. Both of the transmitted and demodulated data are recorded to be compared in ADS software by berMC component. In both setups I and II, for 3.1 Mbits, the number of errors is zero, which means that the BER is less than 10^{-5}.

In the next step, a 2^5-1 pseudorandom bit stream with DR of 2.5 Mbps is transmitted and the PDL and PTE are measured. The PDL is defined as follows:

$$PDL = \frac{1}{NT}\int_0^{NT}\frac{V^2}{R_L}dt \tag{13}$$

where V is the received FSK waveform (V_{RL} in Fig. 11), T is the period, and N is the number of periods. To have a reasonable average PDL, N must be kept as large as possible. The PTE is defined as follows:

$$PTE = \frac{PDL}{V_{cc}I_c + Loss_{Drv.}} = \frac{PDL}{PDL + Loss_{PA} + Loss_{Link} + Loss_{Mod.} + Loss_{Drv.}} \tag{14}$$

where $Loss_{Drv.}$ is the dissipated power in gate drivers (drivers 1 and 2 in Fig. 11), and $V_{cc}I_c$ is the sum of PDL, the dissipated powers in power amplifier ($Loss_{PA}$), inductive link ($Loss_{Link}$), and modulator ($Loss_{Mod.}$). It is worth mentioning that the power supply of drivers 1 and 2 in Fig. 11 is equal to 5 V, and the modulator is supplied with the main source V_{cc} (3 V) in Fig. 11. In biomedical implants, demodulator must be implemented on-chip, which makes it to have very low power dissipation and almost negligible effect on PTE. For this reason, the power dissipation of demodulator implemented with COTS products is not included in relation (14). When a pseudorandom bit stream with 2.5 Mbps DR is transmitted, the measured PDL and PTE (based on relation (14)) in setup I are 57.4 mW and 48.4%, respectively. Also, the PDL and PTE in setup II are 48.2 mW and 38.8%, respectively. In these measurements, the separation of PCB coils is kept as 6 mm.

It is worth mentioning that the reported efficiencies in section 3 are only related to the inductive link (Fig. 3) and the factors limiting the efficiency are the coupling coefficient of PCB coils $L_{1,2}$ as well as the AC resistance of the PCB coils and solenoids. However, in FSK-modulated power and data transmitter of Fig. 11, as shown in relation (14), the power dissipation of power amplifier, gate drivers 1 and 2 in Fig. 11, and the modulator are also taken into account. In Table 3, the measured power dissipation of different parts in transmitter is reported for a separation of 6 mm between the PCB coils in setup 1 and setup 2 during the transmission of pseudorandom bit stream with data rate of 2.5 Mbps. According to Table 3, the power dissipation of modulator implemented with COTS products is considerable. A CMOS on-chip implementation of modulator can make its power dissipation negligible (0.49 mW as reported in section 4), and thus, improves the PTE. However, the power dissipation of COTS modulator is taken into account in this paper.

As in previous works, the power dissipation of demodulator implemented with COTS products is not included in this paper because in biomedical implants, the demodulator must be implemented on-chip with CMOS technologies, which makes it to have low power dissipation (0.41 mW as reported in section 4) and negligible effect on PTE.

In the next step, we have changed the separation of PCB coils and measured the PTE and PDL in both setups I and II (Fig. 16). During this measurement, data is transmitted with DR of 2.5 Mbps. For both setups, since PA is tuned for separation of 6 mm, maximum PTE occurs at this point. By changing the separation, reflected impedance from secondary to primary is changed, which makes the transmitter untune and reduces

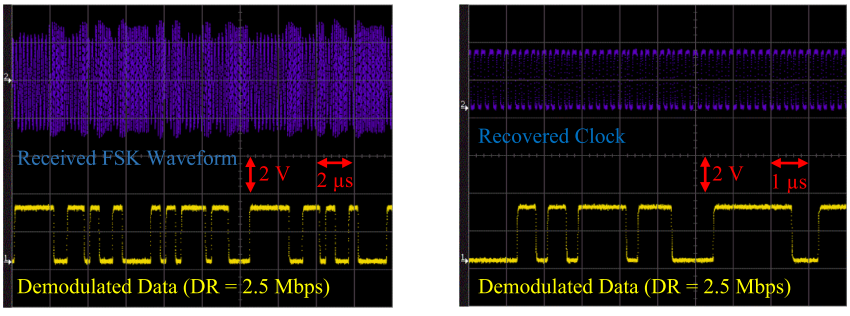

Fig. 15. Measured received FSK waveform, demodulated data and recovered clock at DR of 2.5 Mbps in setup I.

Table 3
Sources of power dissipation in transmitter for a separation of 6 mm between PCB coils in setup 1 and setup 2 (Data Rate = 2.5 Mbps).

Sources of Power Dissipation	Measured Power Dissipation (mW)	
	Setup I (Interface: Air)	Setup II (Interface: Beef Ribs + Silicone)
Power Amplifier and Inductive Link ($Loss_{PA} + Loss_{Link}$)	35.1	49.9
Driver1 + Driver2 in Fig. 11 ($Loss_{Drv.}$)	7.4	7.4
Modulator ($Loss_{Mod.}$)	18.7	18.7

the PDL and PTE. In setup II, in order to be able to reduce the separation to 5 mm, thickness of silicone layer is reduced to 0.5 mm in both coils. For other separations, the silicone layer is kept as 1 mm. Also, thickness of beef ribs in all separations is 4 mm. It should be noted that the decrease in PTE of setup II compared to setup I is due to the reduction of coupling coefficient caused by 4 mm beef ribs between the coils.

The summary of this work is reported in Table 4 to provide a comparison with other state-of-the-art counterparts. The PTEs of our work are based on relation (14) and are measured during the transmission of pseudorandom bit stream with DR of 2.5 Mbps. For the reason already explained, the power dissipation of demodulators implemented with COTS products are excluded in PTEs of all entries in Table 4. It is worth mentioning that we have not implemented the rectifier. An efficient implementation of the rectifier requires its implementation in CMOS process. All of the reported PTEs in Table 4 are without considering the rectifier, and they are measured with an equivalent resistor connected to the secondary side of the inductive link.

In [11], only the power dissipation of inductive link is considered in PTE and the real PTE is less than 24%. In fact, in [11], the delivered power to the input of inductive link is considered as the input power and the dissipated power in PA is not taken into account. This statement is also valid in [35]. In our implemented transmitter, since the secondary side of transmitter has two resonance frequencies, the PTE is considerably improved compared to [10] and [11].

In biomedical implants, tissue absorption increases with the carrier frequency. Therefore, data rate to carrier frequency (DRCF) ratio is an important parameter, and higher DRCF ratio means that the required DR can be achieved with lower carrier frequency. In terms of DRCF ratio, this work has superior performance in comparison with [30–33] and [35]. Although higher DRCF ratio has been achieved in [34,36], they have not implemented the demodulator and the data is not demodulated at the receiver side. So, no BER has been reported in [34,36]. As a matter of fact, there is a trade-off between efficiency and DR when the same inductive link is used for power and data transmission. Therefore, in order to make a quantitative comparison with state-of-the-art counterparts, the following figure-of-merit (FoM) is used [36]:

$$FoM_1 = (DR/f_c) \times PTE \tag{15}$$

where DR/f_c is the same as DRCF ratio. In terms of FoM_1, this work has better performance compared to [10,11,31,32], and [35]. Recently, a new FoM has been proposed in [37] as:

$$FoM_2 = \sqrt[3]{(DR^2/f_c)} \tag{16}$$

where FoM_2 is measured in $(Mbps^2/MHz)^{1/3}$. As a general rule, increasing f_c may increase DR, while increasing f_c makes it harder to obtain a high FoM_2. So, DR^2 is utilized instead of DR in (16). Cubic root reveals important variations in FoM_2 among transmitters in Table 4. In terms of FoM_2, this work has superior performance in comparison with [10] and [30–36].

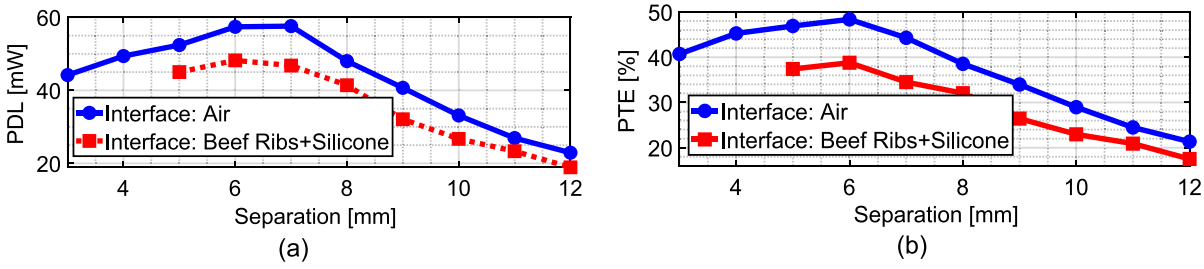

Fig. 16. Measured PDL and PTE of transmitter for DR of 2.5 Mbps and different separations in setup I and setup II. (a) PDL, (b) PTE.

Table 4
Comparison with previous published works.

Ref.	Mod.	Frequency [MHz]	DR [Mbps]	DRCF Ratio	Separation [mm]	Physics	BER	PDL [mW]	PTE [%]	FoM_1	FoM_2
TCAS-I'04 [11]	FSK	5&10	2.5	0.333	5	Air	10^{-5}	~ 5	$< 24^{a,b}$	$< 8^{b}$	0.94
SJ'18 [10]	FSK	2&4	1	0.333	6	Air	10^{-5}	126	25	8.32	0.69
TBE'12 [30]	FSK	5	1.25	0.25	–	Air	–	–	–	–	0.68
TCAS-I'18 [31]	ASK	10	1	0.1	6	Air	10^{-5}	–	52^{c}	5.2	0.46
TPE'21 [32]	ASK	10	2	0.2	10	Air	10^{-6}	35	64.6	12.92	0.74
TBCAS'22 [33]	ASK	$1\&13.56^{d}$	1	0.074	–	Air	1.3×10^{-3}	–	–	–	0.42
TCAS-I'15 [34]	ASK	0.125	0.0625	0.5	–	Air	–	–	–	–	0.31
TCAS-I'20 [35]	CWM	10	1.66	0.166	–	Air	–	–	$< 40^{b,e}$	$< 6.64^{b}$	0.65
TCAS-II'22 [36]	SCM	1	0.5	0.5	–	Air	–	32.3	$< 61^{f}$	$< 30.5^{f}$	0.63
This Work	**FSK**	**5&10**	**2.5**	**0.333**	**6**	**Air**	$\mathbf{10^{-5}}$	**57.4**	**48.4**	**16.12**	**0.94**
This Work	**FSK**	**5&10**	**2.5**	**0.333**	**6**	**Tissue**	$\mathbf{10^{-5}}$	**48.2**	**38.8**	**12.92**	**0.94**

a. Taken from Fig. 11(c) of [11]. 24% is the average of inductive link efficiencies at 5 MHz and 10 MHz for coil separation of 5 mm. **b**. This PTE is without dissipations in PA and gate driver of PA, and is related to inductive link, only. So, the real PTE of [11] and [35] are less than 24% and 40%, respectively. **c**. Taken from Fig. 10(c) of [31] for coil separation of 6 mm. **d**. Separate links for power and data (1 MHz for power and 13.56 MHz for data). **e**. Taken from Fig. 8 of [35]. 40% is the maximum simulated efficiency of inductive link for n = 6 (1.66 Mbps is achieved with n = 6). **f**. PTE of 61% is without dissipation in gate driver of PA. So, the real PTE of [36] is less than 61%.

6. Conclusion

In this paper, an efficient wideband inductive link with two resonance frequencies has been presented. Circular shaped PCB coils and solenoids with winding diameter of 3.22 mm and winding length of 9.46 mm have been used as the main coils and compact inductances, respectively. These dimensions make the link suitable for applications with limited implant space. Using the dual-resonance link, an improved efficiency FSK-modulated class-E transmission link is proposed and its performance is measured in two different setups. In setup I, the intermediate interface of PCB coils is 6 mm air gap. In setup II, in order to mimic the condition of cochlear implants, a 4 mm beef ribs is used as the interface between the coils. Also, the medical-grade silicone with thickness of 1 mm is used as a coating layer for both of PCB coils. In both setups, a pseudorandom bit stream with DR of 2.5 Mbps is transmitted to measure the PDL, PTE, and BER of power and data transmitter. In setup I, the measured PDL and PTE are 57.4 mW and 48.4%, respectively. In setup II, the measured PDL and PTE are 48.2 mW and 38.8%, respectively. The existence of two resonance frequencies at the secondary side of the link increases the PTE, considerably. The measured BER in both setups is less than 10^{-5}.

Declaration of Competing Interest

The authors declare that they have no known competing financial interests or personal relationships that could have appeared to influence the work reported in this paper.

Data availability

No data was used for the research described in the article.

Acknowledgement

This work has been financially supported in part by Iran National Science Foundation (INSF) under the contract number of 99011612.

References

[1] Bagheri A, Erfanian A, Abrishamifar A. Automatic tuning of the Class E power amplifier applied in inductive links during coil separation variations. AEU-Int J Electronics and Commun Sep. 2020;124:153337.
[2] Murliky L, Porto RW, Brusamarello VJ, de Sousa FR, Triviño-Cabrera A. Active tuning of wireless power transfer system for compensating coil misalignment and variable load conditions. AEU-Int J Electronics and Commun May 2020;119:153166.
[3] Kar DP, Biswal SS, Sahoo PK, Nayak PP, Bhuyan S. Selection of maximum power transfer region for resonant inductively coupled wireless charging system. AEU-Int J Electronics and Commun Feb. 2018;84:84–92.
[4] Karimi MJ, Schmid A, Dehollain C. Wireless power and data transmission for implanted devices via inductive links: a systematic review. IEEE Sens J Mar. 2021;21(6):7145–61.
[5] Yang X, et al. A cost-effective implementation of independent data and power transmission channels in wireless power transfer systems. IEEE Trans Circuits and Syst II: Express Briefs Mar. 2022;69(3):1532–6.
[6] Kim JG, Wei G, Kim MH, Ryo HS, Ri PC, Zhu C. A splitting frequencies-based wireless power and information simultaneous transfer method. IEEE Trans Circuits and Syst I: Regular Papers Dec. 2018;65(12):4434–45.
[7] Wang G, Wang P, Tang Y, Liu W. Analysis of dual band power and data telemetry for biomedical implants. IEEE Trans Biomedical Circuits and Syst Jun. 2012;6(3):208–15.
[8] Simard G, Sawan M, Massicotte D. Novel coils topology intended for biomedical implants with multiple carrier inductive link. IEEE Int. Symp. Circuits and Systems (ISCAS) May 2009:537–40.
[9] Jow UM, Ghovanloo M. Optimization of data coils in a multiband wireless link for neuroprosthetic implantable devices. IEEE Trans Biomedical Circuits and Systems Oct. 2010;4(5):301–10.
[10] Ahmadi MM, Ghandi S. A Class-E power amplifier with wideband FSK modulation for inductive power and data transmission to medical implants. IEEE Sens J Sept. 2018;18(17):7242–52.
[11] Ghovanloo M, Najafi K. A wideband frequency-shift keying wireless link for inductively powered biomedical implants. IEEE Trans Circuits and Systems I: Regular Papers Dec. 2004;51(12):2374–83.
[12] Kung ML, Lin KH. Enhanced analysis and design method of dual-band coil module for near-field wireless power transfer systems. IEEE Trans Microwave Theory and Techniques Mar. 2015;63(3):821–32.
[13] Kim JG, Wei G, Kim MH, Ryo HS, Zhu C. A wireless power and information simultaneous transfer technology based on 2FSK modulation using the dual bands of series–parallel combined resonant circuit. IEEE Trans Power Electronics Mar. 2019;34(3):2956–65.
[14] Schormans M, Valente V, Demosthenous A. Practical inductive link design for biomedical wireless power transfer: a tutorial. IEEE Trans Biomed Circuits and Systems Oct. 2018;12(5):1112–30.
[15] Knight DW. An introduction to the art of solenoid inductance calculation with emphasis on radio-frequency applications. Feb. 2016; http://g3ynh.info/zdocs/magnetics/part_1.html.
[16] Stroobandt SY. The effective diameter of a single-layer helical coil inductor as a function of the proximity factor. Jul. 2007; https://hamwaves.com/inductance/doc/effective_diameter.pdf.
[17] Knight DW. Selonoid impedance and Q. Jan. 2016; http://g3ynh.info/zdocs/magnetics/solenz.html.
[18] Jow UM, Ghovanloo M. Design and optimization of printed spiral coils for efficient transcutaneous inductive power transmission. IEEE Trans Biomed Circuits and Syst Sept. 2007;1(3):193–202.
[19] Knight DW. The self-resonance and self-capacitance of solenoid coils: applicable theory, models and calculation methods. May 2016; http://g3ynh.info/zdocs/magnetics/appendix/self-res.html.
[20] Lin JC. Computer methods for field intensity predictions. CRC Handbook of Biological Effects of Electromagnetic Fields, CRC Press, ch 1986;2:273–313.
[21] Rezaeiyan Y, Zamani M, Shoaei O, Serdijn WA. Mixed-signal IC with pulse width modulation wireless telemetry for implantable cardiac pacemakers in 0.18-μm CMOS. IEEE Trans Biomed Circuits and Systems Jun. 2018;12(3):589–600.
[22] Campi T, Cruciani S, Maradei F, Montalto A, Musumeci F, Feliziani M. EMI in a cardiac implantable electronic device (CIED) by the wireless powering of a left ventricular assist device (LVAD). IEEE Trans Electromagnetic Compatibility Aug. 2021;63(4):988–95.
[23] Trigui A, Hached S, Ammari AC, Savaria Y, Sawan M. Maximizing data transmission rate for implantable devices over a single inductive link: methodological review. IEEE Rev Biomed Eng Oct. 2018;12:72–87.
[24] Zeng FG, Rebscher S, Harrison W, Sun X, Feng H. Cochlear implants: system design, integration, and evaluation. IEEE Rev Biomed Eng Nov. 2008;1:115–42.
[25] Qian XH, et al. Design and In vivo verification of a CMOS bone guided cochlear implant microsystem. IEEE Trans Biomed Eng Nov. 2019;66(11):3156–67.
[26] Jung LH, Byrnes-Preston P, Hessler R, Lehmann T, Suaning G, Lovell NH. A dual band wireless power and FSK data telemetry for biomedical implants. Int. Conf. of IEEE Engineering in Medicine and Biology Society, Aug. 2007, pp. 6596–6599.
[27] Oltulu P, Ince B, Kokbudak N, Findik S, Kilinc F. Measurement of epidermis, dermis, and total skin thicknesses from six different body regions with a new ethical histometric technique. Turkish J Plastic Surgery Apr. 2018;26(2):56–61.
[28] Gabriel S, Lau R, Gabriel C. The dielectric properties of biological tissues: II. measurements in the frequency range 10 Hz to 20 GHz. Phys Med Biol Nov. 1996;41(11):2251–69.
[29] Jow UM, Ghovanloo M. Modeling and optimization of printed spiral coils in air, saline, and muscle tissue environments. IEEE Trans Biomedical Circuits and Syst Oct. 2009;3(5):339–47.
[30] Rush AD, Troyk PR. A power and data link for a wireless-implanted neural recording system. IEEE Trans Biomedical Engineering Nov. 2012;59(11):3255–62.
[31] Navaii ML, Sadjedi H, Sarrafzadeh A. Efficient ASK data and power transmission by the class-E with a switchable tuned network. IEEE Trans Circuits and Systems I: Regular Papers Oct. 2018;65(10):3255–66.
[32] Ahmadi MM, Pezeshkpour S, Kabirkhoo Z. A high-efficiency ASK-modulated class-E power and data transmitter for medical implants. IEEE Trans Power Electronics Jun. 2021;37(1):1090–101.
[33] Chen Y, Liu Y, Li Y, Wang G, Chen M. An energy-efficient ASK demodulator robust to power-carrier-interference for inductive power and data telemetry. IEEE Trans Biomed Circuits and Syst Feb. 2022;16(1):108–18.
[34] Lee EK. A discrete controlled fully integrated class E coil driver with power efficient ASK modulation for powering biomedical implants. IEEE Trans Circuits Syst I, Reg Papers, Jun 2015;62(6):1678–87.
[35] Trigui A, et al. Generic wireless power transfer and data communication system based on a novel modulation technique. IEEE Trans Circuits and Systems I, Regular Papers Nov. 2020;67(11):3978–90.
[36] Dehghan K, Shoaei O, Ashtiani SJ. A Class-E power and data transmitter with improved data rate to carrier frequency ratio for medical implants. IEEE Trans Circuits and Systems II: Express Briefs Jun. 2022;69(6):2692–6.
[37] Barbruni GL, et al. A 20 Mbps, 433 MHz RF ASK transmitter to inductively power a distributed network of miniaturised neural implants. IEEE Int Symp Medical Measurements and Aplications 2021:1–6.